PERGAMON

International Journal of Solids and Structures 37 (2000) 3901–3918

INTERNATIONAL JOURNAL OF SOLIDS and STRUCTURES

www.elsevier.com/locate/ijsolstr

A mechanical model for the elastic–plastic behavior of metallic bars

Maurizio Froli[a], Gianni Royer-Carfagni[b,*]

[a]*Dipartimento di Ingegneria Strutturale dell'Università di Pisa, Italy*
[b]*Dipartimento di Ingegneria Civile dell'Università di Parma, Parco Area delle Scienze 181/A, 43100, Parma, Italy*

Received 23 May 1998; received in revised form 19 March 1999

Abstract

A simple mechanical model, which consists of a particular assemblage of elementary units composed of elastic springs and frictional sliding blocks, appears suitable for describing the various aspects of the elastic–plastic behavior of steel bars in standard tensile tests: oscillations in the average stress–strain curve, the distinction between local and global responses, instability due to the transition from an upper to a lower yield point, the spread of plastic deformation, strain-hardening behavior, elastic unloading and the influence of loading-device stiffness.

1. Introduction

In the words of J. F. Bell (1973), from the beginning of the 19th Century up to today 'nearly every decade has seen commentary on the phenomenon of discontinuous plastic deformation'. This is the phenomenon easily recognizable by measuring the corresponding axial load in any mild steel bar when it is pulled by means of a testing-machine, at a prescribed relative displacement of the clamping jaws (i.e., imposed deformation test). Although a well-defined plastic *plateau* usually results, by looking more closely at a typical mean-stress vs mean-strain diagram like that in Fig. 1a, it is evident that yielding is actually a 'pseudo-equilibrium' state, in which the mean stress exhibits irregular oscillations around a nearly constant average value. Serrated deformations can also be observed in metals when they are subjected to dead-weight loading: the strain progresses in sudden jumps rather than uniformly over time even when the loading rate is kept constant and usually, the lower the loading rate is, the more

* Corresponding author. Tel.: +39-521-905922; fax: +39-521-905924.
E-mail address: royer@parma1.eng.unipr.it (G. Royer-Carfagni).

0020-7683/00/$ - see front matter
PII: S0020-7683(99)00069-4

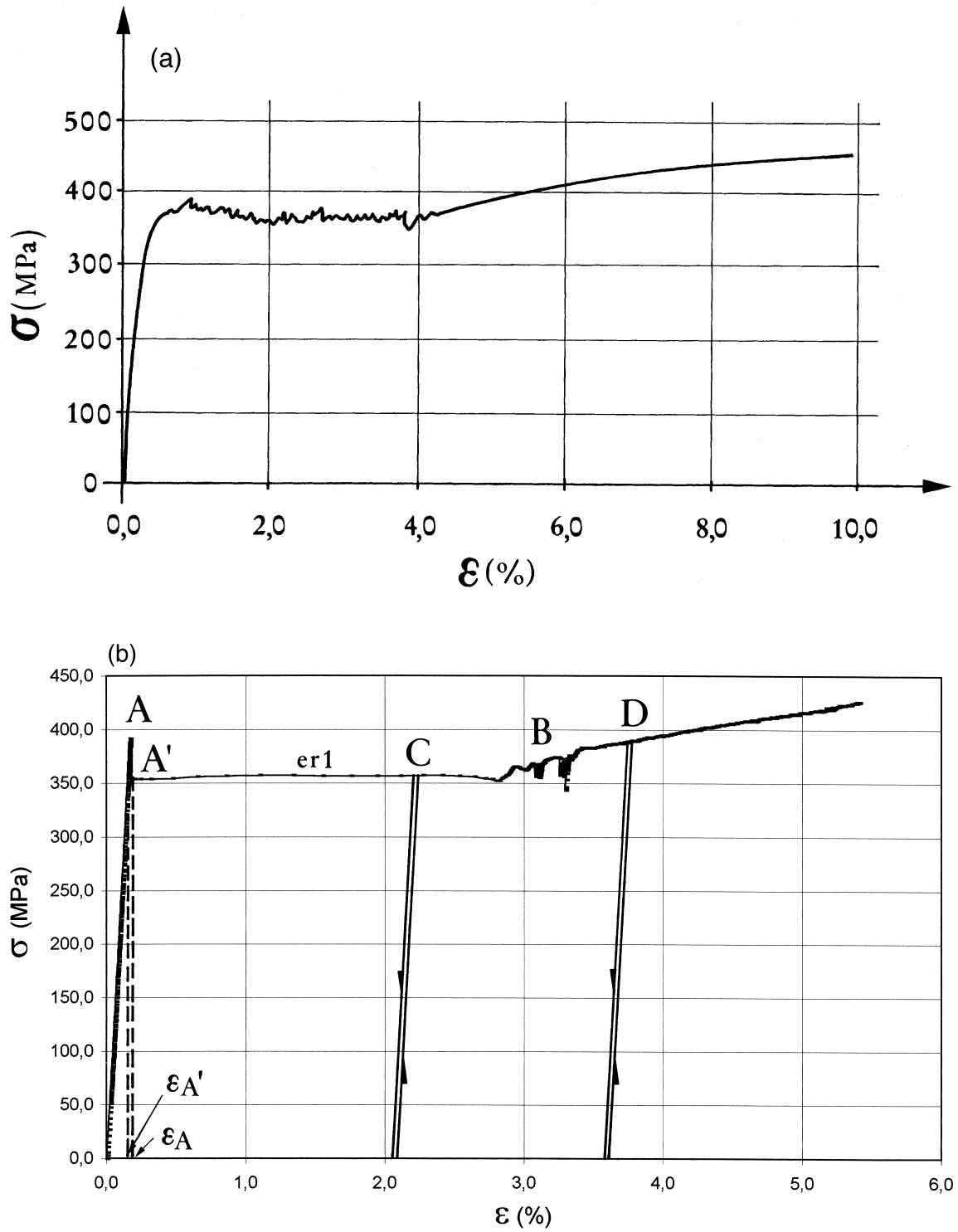

Fig. 1. Typical σ–ε diagrams for an imposed-deformation tensile test. (a) averaged response; (b) local response.

discontinuous the steps are. Moreover, the phenomenon is more pronounced in low than in high-purity metals (Bell, 1973, Section 4.31).

Attempts at explaining such behavior follow essentially two kinds of reasoning. By one way of thinking, the oscillations can be attributed to the influence of the testing machine, whereas the other approach views them as the reflection of an internal material instability, irrespective of the loading device. Support for the latter theory comes from commentaries on the experimental investigations of Duleau (1813), Savart (1837), Masson (1841), Rosenhain and Archbutt (1912), Portevin and Le Chatelier (1923), Hanson and Wheeler (1931), while the former rationale was sustained first by Wertheim (1844), then by most scholars of the early 20th Century and more recently by Lempriere (1962) who, in particular, tried to mathematically demonstrate the dynamic interaction between the velocity of a specimen's plastic deformation and the inertia of the testing machine.

Nowadays, it is commonly accepted that such oscillations cannot be considered simply a secondary effect induced by the loading device. However, it has, at the same time, become equally clear that testing conditions, such as specimen temperature, speed of imposed deformation and, consequently, testing-machine stiffness, can greatly effect the apparent material response (Korber, 1926; Schulz and Buchholtz, 1926; Elam, 1938; Welter and Gockowski, 1938; Davis, 1938; Manjoine, 1944). A decisive contribution in this direction came from the experiments first performed in 1937 by Siebel and Schwaigerer (1937–1938) who in order to explore the influence of testing-device stiffness on the shape of the σ–ε diagrams, inserted an elastic spring in series with the test bar. They found that the drop in the stress–strain curve at yielding diminished progressively and finally vanished when the spring's stiffness was decreased. These results were later confirmed by Miklowitz (1947), who found that *even the stress oscillations at yielding may disappear* at room temperature, if the stiffness of the spring is sufficiently low.

Recently, the authors (Froli and Royer-Carfagni, 1997, 1999) have underscored the need to introduce a distinction between an 'averaged' and a 'local' material response. These can be obtained by considering the averaged and the local strain, the former traditionally defined as the ratio between the relative displacement of the bar's ends and its initial length, while the second was measured by short resistance strain gauges placed at regular intervals longitudinally along the bar axes. Figs. 1a and 1b illustrate two such typical responses in graphs correlating the average stress σ with either the averaged (Fig. 1a) or the local (Fig. 1b) strain. These results are relative to one of the tests reported in Froli and Royer-Carfagni (1999) on cylindrical mild-steel bars, 16 mm in diameter, on which the local measurements were performed through 6 mm-long, high-performance (10% allowable strain) gauges. The graphs are interrupted at the beginning of strain hardening, before which necking-related phenomena are significant; hence, the true stress can be considered practically equal to σ, i.e., the tensile force per unit of the bar's undistorted cross-sectional area.

Although the local relations in Fig. 1b are similar to those obtained by measuring averaged quantities as in Fig. 1a, some substantial differences are clearly present. The most evident is that in the local response *hardly any oscillations at yielding can be observed*. A further distinction is in the transition between the elastic and yielding periods. This transition is smooth, but curly in the average-value graph; sharp and straight in the local diagram where, after reaching point A, the mean stress abruptly joins the plastic *plateau* at point A′, with no tendency to chamfer (Fig. 1b). After C. von Bach (Nadai, 1950, Section 19.1), point A is traditionally called the upper-yield point (*Oberestreckgrenze*) and A′ the lower-yield point (*Unterestreckgrenze*). It should also be noted that the upper and lower-yield points tend to coincide when the specimen is released and successively reloaded, regardless of whether the unloading be in the middle of the local plastic plateau (point C in Fig. 1b), or in the strain-hardening branch (point D, Fig. 1b).

Other peculiarities are evidenced in Fig. 2, which presents, as a function of time, the mean-stress and local-strain histories measured by eight resistance strain gauges (Froli and Royer-Carfagni, 1997) numbered according to their placement along the bar's axis. The ordered sequence of strain jumps

recorded by the gauges provides evidence that localized plastic distortions do not nucleate randomly, but slowly advance as a plastic wave in a precise order throughout the bar. This is usually referred to as *McReynolds' slow wave*, in honor of the scientist, McReynolds (1949), who first recognized the progression of plastic deformation in dead-weight testing in the simultaneous recordings of four wire gauges uniformly spaced along the specimen's axis (see also Dillon, 1966; Sharpe, 1966; Bell, 1968, Section 1.31; Schmidt, 1995).

The present paper represents an attempt to interpret the complex phenomena occurring in the tensile response of steel bars through a simple mechanical model which, in our opinion, could be the starting point for derivation of a more complete, 3D, continuum mechanics model. A similar issue was previously addressed by a number of authors, among whom Müller and Villaggio (1977) who, building upon Ericksen's (1975) pioneering work, conceived of a plastic body as composed of hypothetical arrays of snap-springs. Such constructs were heuristic devices analogous to the well-known dash-pots simulating internal friction in a viscous body: just as a dash-pot represents the effect of momentum transfer between a group of molecules, snap-springs are indicative of the effect of loading on dislocation movements. It is also similar in kind to the well-known dynamic system of Carlson and Langer (1989), consisting of an elastically coupled chain of masses mechanically conceived of as rigid blocks. The chain is in contact with a moving rough surface and driven persistently toward slipping instability, which is obtained by introducing a non-linear, velocity-dependent friction law at the interface between the blocks and moving surface. A more refined model has recently been proposed by Burns (1994) and shown to be able to explain the onset of discontinuous plastic flow in metals at cryogenic temperatures. This phenomenon consists of sudden load drops associated with local elongation following a sudden local increase in temperature. In a heat bath at a temperature of a few Kelvin degrees, thermodynamic

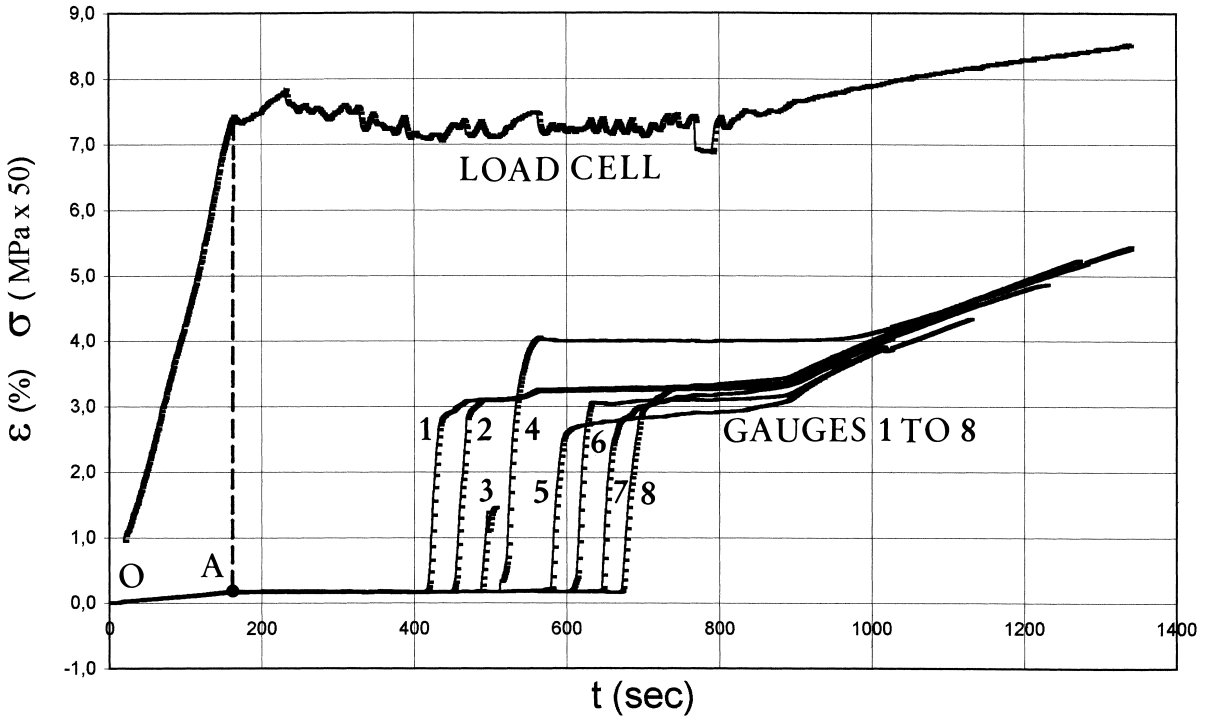

Fig. 2. Mean-stress and local-strain histories for a tensile test.

balance may play a decisive role: once one assumes that plastic flow is associated to heat production, the yielding of one particle produces a drastic localized temperature change with respect to the surrounding atmosphere, which can also radically affect the material's local behavior. However, it is our expectation that at room temperature such effects are not decisive, whereas other phenomena, such as the possibility that the yielding of one particle influences the others closest to it, do become critical.

In our interpretation, a metallic bar can be conceived of as an assemblage of elementary constituent units consisting of the combination of linear springs and friction-sliding blocks, these latter activated by the eventual breakage of a retaining tooth. It will be shown that the response of the single unit can reproduce the local material behavior plotted in Fig. 1b. Afterwards, in order to reproduce the non-local interaction between material particles at yielding, a particular assemblage of three arrays of these elementary constituents will be introduced. This arrangement is shown to be able to completely describe and interpret the global response in Fig. 1a, as well as the local-strain histories depicted in Figs. 1b and 2. In addition, by inserting springs of different stiffness in series with the whole assemblage, the possible influence of the loading device will be discussed.

2. The model

The plastic-bar unit element considered here is that represented in Fig. 3. It is an assemblage of a

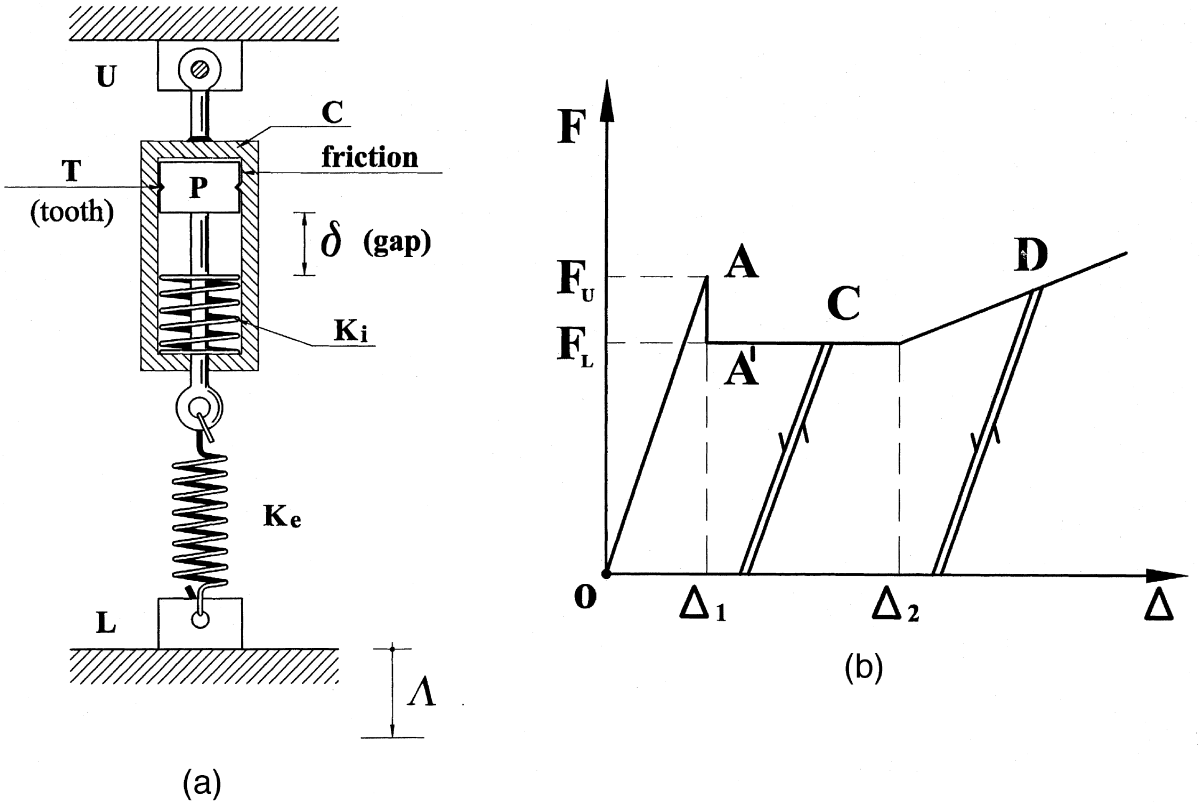

Fig. 3. The constituent element and local F–Δ relations.

linear spring of stiffness K_e in series with a module consisting of a rigid cylinder C connected in parallel to another linear elastic spring of stiffness K_i and a friction-sliding piston P. We suppose that friction sliding occurs only when the drag force equals the value F_L, though block P is initially confined to its resting position by a retaining tooth T, which breaks when subjected to a force $F_U > F_L$.

By assuming that one end of the unit element is fixed, while the other is subjected to a given displacement Δ (Fig. 3), we can calculate the force F offered by the restraints as the displacement Δ is increased. At the outset, the retaining tooth T exerts a much stiffer constraint than frictional contact, which requires relative motion between P and C in order to develop its full bearing capacity F_L . Thus, as long as

$$\Delta < \Delta_1 = \frac{F_U}{K_e}, \tag{1}$$

the piston P is blocked, and the external spring alone carries the load. Consequently, the F–Δ graph presents a first linear branch with slope K_e (Fig. 3b). When Δ increases and the retaining tooth breaks, P then slides a certain amount and releases spring K_e until it exerts a force equal to F_L, the greatest allowed by friction. The result is that point $A \equiv (\Delta_1, F_U)$ in Fig. 3b suddenly drops to point A' at coordinates (Δ_1, F_L). Subsequent relative displacement produces further sliding of piston P at constant force $F = F_L$. This phase, corresponding to the *plateau* in Fig. 3b, lasts until the initial gap δ has been completely closed, that is, up to the value

$$\Delta = \Delta_2 = \frac{F_L}{K_e} + \delta. \tag{2}$$

At this point, the internal spring K_i comes in contact with the piston P, and from here on the displacement Δ satisfies a linear relation of the form

$$\Delta = \Delta(F) = \frac{F}{K_e} + \delta + \frac{F - F_L}{K_i}. \tag{3}$$

This corresponds to the 'strain hardening' linear branch of Fig. 3b, which consequently presents slope

$$K^{SH} = \frac{dF}{d\Delta} = \frac{K_e K_i}{K_e + K_i}. \tag{4}$$

Fig. 3b illustrates what happens if unloading is performed at, say, point C, in the middle of the *plateau*. If the force F decreases, the piston P cannot slide any further. Consequently, unloading results in the release of spring K_e, and the stress–strain diagram follows a path parallel to the initial linear branch OA. Subsequent reloading returns along the same path, but *no drop in stress*, like the one between points A and A', occurs because the retaining tooth T has already been broken. The same holds if unloading is performed at, say, point D in the 'strain-hardening' branch, because in this case as well, the piston P does not slide when the load is released, and the main contribution once again comes from the stiffness K_e. This time, however, the internal spring K_i remains compressed by the force $F = F_D - F_L$ (F_D is the axial force at point D in Fig. 3b), compensated by the frictional contact between cylinder C and piston P as an internal self-equilibrating action (of course, this is true until $| F_D - F_L | < F_L$). This is in agreement with the thermo-mechanical considerations of G. I. Taylor, W. S. Farren and H. Quinney (Nadai, 1950, p. 55), who state that elastic energy remains stored in plastically bent lamellae in distorted crystal grains of strain-hardened metals.

The unit defined in the foregoing is representative of *local* behavior and can be interpreted at the microstructural level in terms of the theory of dislocation and plastic flow in crystals (Cottrell, 1961,

Section 13). According to the classical explanation for the sharp yielding point in ferrous alloys (Cottrell, 1961), solute atoms, which are able to migrate through the crystal under the action of thermal fluctuations, will, in the presence of a dishomogeneous field such as the stress field of a dislocation, drift towards those places where their energy state is lowest. Thus, the starting scenario of an unyielded portion of an alloy is the segregation of solute atoms around stationary dislocations. Since the migration of solute atoms takes much longer than the movement of a dislocation, in the presence of an external stress field, dislocations will initially remain anchored to the surrounding atmosphere produced by the solute atoms. If a long enough time is allowed during the tests for the migration of solute atoms to occur, creep effects may become important. However, if the loading speed is high enough to allow discounting such an effect, the material could exist in either of two conditions: in the first, the *unyielded* or strain-aged condition, the dislocations are anchored and deformation is purely elastic; in the second, the *overstrained* condition, dislocations are free to move under applied stress and thus produce plastic deformations.

In the model described in Fig. 3, the breakage of the retaining tooth marks the transition from the unyielded to the overstrained condition. In line with the classical theory of Peierls and Nabarro (Cottrell, 1961, Sections 6.1–6.2), we have further supposed that once the anchoring link has been broken, the dislocation can migrate at a critical force, F_L. This critical force accompanying any possible dislocation movement is modeled in Fig. 3 by the frictional constraint between the cylinder and piston, which can slide one over the other precisely at the force F_L. At the microstructural level, it can also be demonstrated that any unloading reduces the drag force on dislocations (Cottrell, 1961, Section 3.3), just like the relative force between piston and cylinder diminishes when the unit is released, regardless of whether the unloading is in the plastic plateau or at the beginning of strain hardening. Since the dislocations remain stuck at their positions, recovery is due entirely to the elasticity of the crystal and consequently occurs along linear paths (Fig. 2b). Similarly, in the model no relative motion is possible between the cylinder and piston, and unloading remains governed by the elasticity of the external spring K_e. It also seems worth noting that the model suggests a new explanation for work hardening.

The next step, fundamental to interpreting the phenomena occurring in tensile bars, is to admit some interaction between the elementary units. Following the indications of some experimental studies (Wertheim, 1844, Sections 19.1–19.2), in particular those of Davis (1938), we surmised that any localized yielding produces a condition equivalent to stress concentration, which can greatly influence the nearest elementary portions. Such behavior can be modeled most simply by considering the bar to be composed of three arrays of elementary units made up of (Fig. 4) two element classes arranged as in Fig. 3. The short ones, with length l, are distinguished by parameters δ, K_i, K_e, F_U, F_L, and the long ones, of length $2\,l$, by representative parameters 2δ, $K_i/2$, $K_e/2$, F_U, F_L. The three arrays, one formed by $(2n + 1)$ short elements and the other two by one short plus n long elements, are connected to each other, as

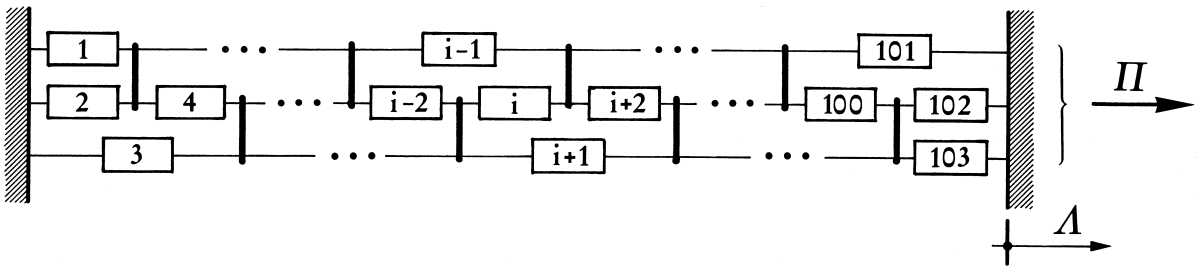

Fig. 4. Schematic representation of the constituent element arrays in the model bar.

represented schematically in Fig. 4. For the sake of illustration, the three arrays have been represented in the figure as one beside the other, though they must be understood as ideally lying in a single line, with no eccentricity, and each transverse connection among four distinct elements must be considered a single node, thus imposing an identical longitudinal displacement on the connected points.

Of course, many other unit arrangements are possible. However, the one in Fig. 4 is likely to be the simplest satisfying an indispensable feature: whenever one element (say, element i in Fig. 4) experiences traction F_U, its retaining tooth breaks, nucleating a distortion which affects the neighboring elements ($i-1$) and ($i+1$). These will consequently be overloaded, developing a chain-reaction which results in the spread of frictional sliding throughout the elementary-unit assemblage, just as in the case of McReynolds' plastic slow wave.

3. Qualitative response of the model

We first consider the case in which the model bar is composed of $2n$ long and $2n+3$ short elementary units, each equal to others of the same kind, arranged as in Fig. 4. In order to better correlate the model to a real case, we consider a metal rod of length L, cross-section A, initial Young's modulus E and strain-hardening modulus E^{SH}. Then, with the same notation as in Figs. 3 and 4, we set

$$l=\frac{L}{2n+1},\quad K_e=\frac{EA/3}{l},\quad K^{SH}=\frac{E^{SH}A/3}{l},$$

$$K_i=\frac{EE^{SH}}{E-E^{SH}}\frac{A/3}{l},\quad F_u=\sigma_y^u\frac{A}{3},\quad F_{L=}\sigma_y^l\frac{A}{3}, \tag{5}$$

where σ_y^u and σ_y^l represent the upper and lower yield stress of the local response in Fig. 1b. Neglecting the units' own weights, we prescribe that the extremities of the model bar are displaced apart by a quantity $\Lambda=\Lambda(t)$ and, like a standard imposed-deformation tensile test in a hard device, we fix the relative displacement velocity $d\Lambda/dt$ of the clamped ends.

If Π is the total reaction offered by the test-machine constraints, the generic ith element will be drawn by $F_i=\Pi/3$ until

$$\frac{\Lambda}{2n+1}<\Delta_1=\frac{F_U}{K_e}, \tag{6}$$

that is, up to $F_i < F_U$. By increasing the relative displacement of the extremities, there exists the possibility that the retaining teeth of all the units break at the same instant, producing a simultaneous sliding of the pistons. However, in order to account for dishomogeneities, we suppose that the resistance of the various retaining teeth differ from one another by an infinitesimal quantity ε. Thus, one tooth breaks first and will produce local release and the nucleation of 'plastic' deformation.

In order to simulate experimental results, we refer to the test reported in Fig. 1, where the specimen presented approximately $L = 50$ cm and $A = 2.01$ cm^2. From the graph in Fig. 1b, we can obtain $E = 2.0\times10^5$ MPa, $E^{SH}=3.33\times10^3$ MPa, $\sigma_y^u=390$ MPa, $\sigma_y^l=358$ MPa (Froli and Royer-Carfagni, 1999).

An assemblage of 50 long and 53 short elementary units, in which the short units have approximately the same length as the strain gauges used in Froli and Royer-Carfagni (1999), has been calibrated by applying Eq. (5) and assuming the above values. In order to reproduce the fact that one tooth breaks first, we have considered one element (the 52nd, according to the numbering in Fig. 4) to have an upper yield point $\bar{\sigma}_y^u=389$ MPa that is slightly lower than the others (390 MPa). The response of the

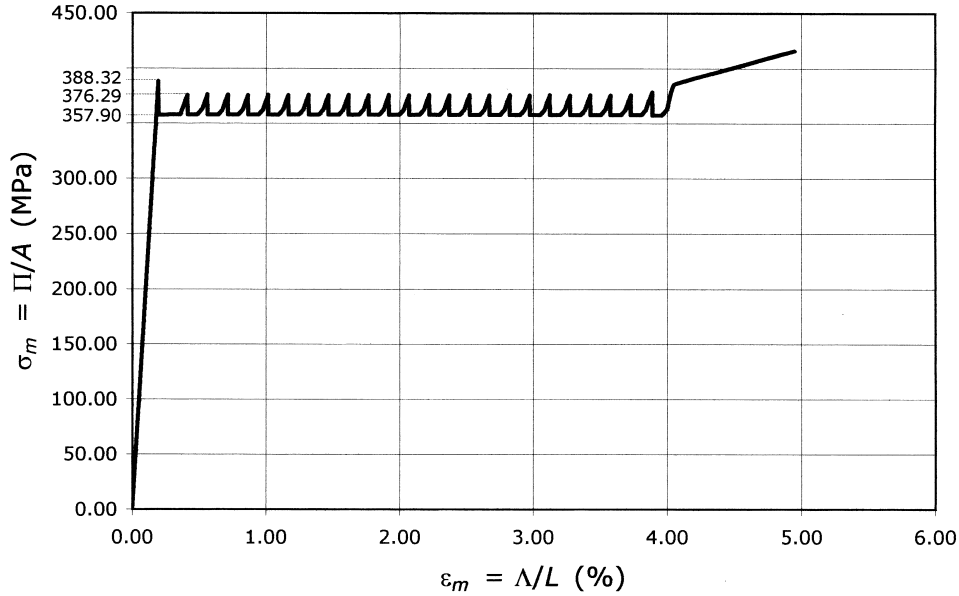

Fig. 5. Average stress–strain diagrams for uniform chain-bar model.

composite system when its extremities (as in the experiment) are displaced apart at a velocity of $d\Lambda/dt = 2$ mm/min was analyzed using an Ansys finite element code utilizing mono-dimensional elements with constitutive laws as in Fig. 3b, assembled according to the scheme in Fig. 4.

Fig. 5 shows the mean reaction-stress Π/A of the clamped edge as a function of the average strain

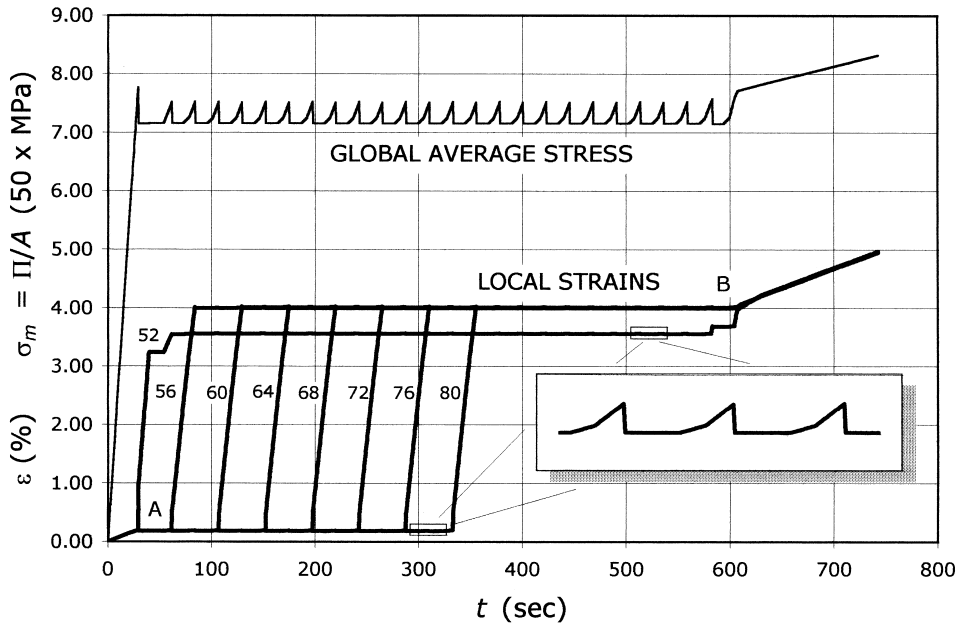

Fig. 6. Local strain for various elements and global average stress as functions of time.

Λ/L. Marked oscillations, due to the aforementioned chain-reaction mechanism, are clearly recognizable. Plastic deformation was verified to actually nucleate at the weakest element and then progress symmetrically.

In order to correlate the model with the output of strain gauges in Fig. 2, we define the local strain ε_i as the relative displacement of the extremities of any given ith element divided by its initial length.

Fig. 6 presents, as a function of the time, the ε_i corresponding to several elements spaced approximately at the same distance as the gauges applied to the real bar. In the first phase, when all elements remain elastic, the diagrams overlap on the first branch OA, which is linear because we have imposed a constant deformation velocity. Plastic deformation nucleated at the weakest unit (n. 52) when $\Pi/A \cong 389$ MPa and affected the nearest six neighboring elements until sliding of the pistons produced a sufficient release of the entire model bar. This release is evidenced by the first drop in the average-stress history, also reported in Fig. 6. Further displacement of the extremities produces additional sliding of the pistons at constant stress until contact with the springs K_i is made, giving rise to a new increase in stress. Inelastic deformation then progresses symmetrically towards both ends. We observe that the peak average stress in the first serration is greater than in the others, despite the fact that plasticity nucleates at a portion containing the weakest element. This is because breakage of a retaining tooth in one constituent produces much greater damage than that artificially introduced by reducing the resistance of the tooth in element n. 52. It should also be noted that, while element n. 52 undergoes a jump in strain, the diagrams relative to the other elements become practically horizontal at point A. More precisely, Fig. 6, which shows a magnification of the pseudo-horizontal branches, reveals small oscillations that match the average-stress history exactly.

The similarity between Figs. 2 and 6 is immediately evident, the main difference being that, in the first case, all the gauge graphs become pseudo-horizontal at point A; a response like that of element 52 is lacking. This is because in a real bar it is impossible to predict where yielding nucleates and to place a strain gauge exactly at that point. However, if this were possible, we would obtain the same trend as in Fig. 6.

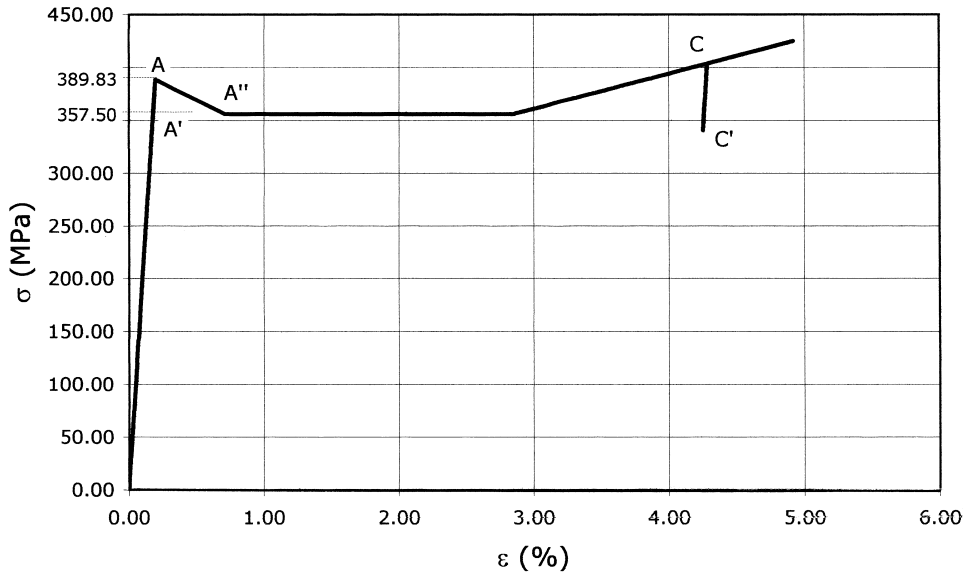

Fig. 7. Local stress–strain diagram for element n. 80.

Fig. 7 shows the local stress–strain curve for one significant element (n. 80). In this graph, branch A-A″-C corresponds to the sudden strain increase in Fig. 6, which is thus revealed as occurring essentially along the *plateau*. The oscillations, evidenced by the magnifications in Fig. 6, can be found in Fig. 7 along two distinct paths: along A-A′, *before* the retaining tooth breaks, and along path C-C′, *after* the jump in deformation. In particular, branch C-C′ corresponds to the situation in which the piston is in contact with the internal spring K_i (Fig. 3), but stuck in this position due to frictional contact with the cylinder. Therefore, at this stage the observed oscillations are due entirely to the elasticity of the external spring K_e. It should also be noted that strain hardening develops, and the representative point rises beyond point C in Fig. 7 only at time $t > 600$ (Fig. 6), that is, only *after* the retaining teeth of all the elements have broken. At this stage, once again all the graphs overlap on a single branch.

Indeed, the local response obtained in tests (Froli and Royer-Carfagni, 1999) was found to differ considerably from one gauge point to the next. In particular, the values E^{SH}, σ_y^u and σ_y^l were found to vary one from the other by the order of 10%, whereas even greater discrepancies occurred in plastic elongation (up to 25%). This effect can be simulated by letting the material properties of the constituent elements vary randomly throughout the bar.

By considering random chains, we obtain the average stress–strain diagram shown in Fig. 8, which resembles Fig. 1a much more closely than Fig. 5.

The corresponding local-strain histories, represented in Fig. 9, are not as uniform as in Fig. 6, though the progression of a slow wave is once again clearly recognizable. This is because failure of any one of the retaining teeth produces overloading of the neighboring elements, which masks all the originally assumed differences. The result is the advancement of an inelastic wave, which in this case, however, produces irregular oscillations because it successively encounters elements whose properties differ one to the next. The strain-hardening phase progresses again only when all the retaining teeth have broken, as revealed in Fig. 9 by the increasing branches of equal slope starting at $t \approx 600$. However, this time the curves do not overlap, as in Fig. 6, because of the differences in the local plastic *plateaux* assumed for the various elements.

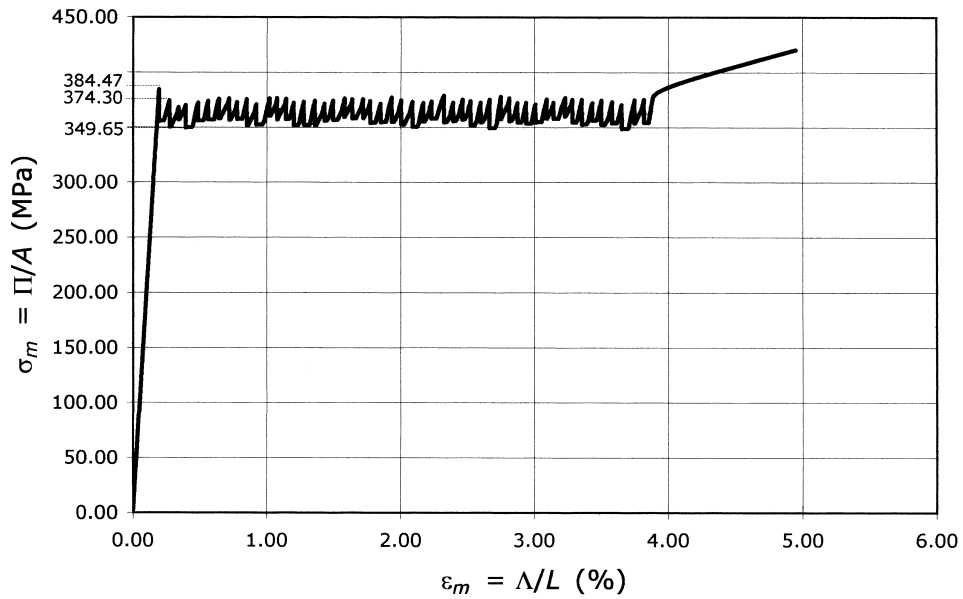

Fig. 8. Average stress–strain diagrams for random chain-bar model.

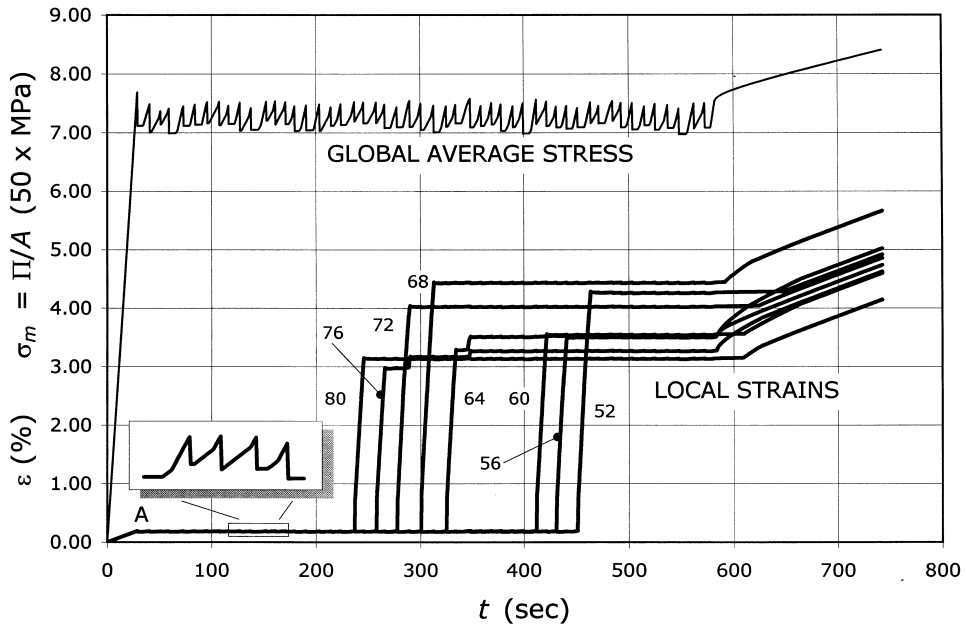

Fig. 9. Local strain for various elements and global average stress as functions of time; random chain.

Another peculiarity of the random-chain model is represented by the spread of the slow wave. Whereas in the uniform-chain model the slow wave advanced symmetrically on both sides, here plastic deformation progresses in a seesaw manner. In fact, due to the heterogeneity, the slow wave advances wherever it encounters lowest resistance. This is confirmed by the number of oscillations in Fig. 8,

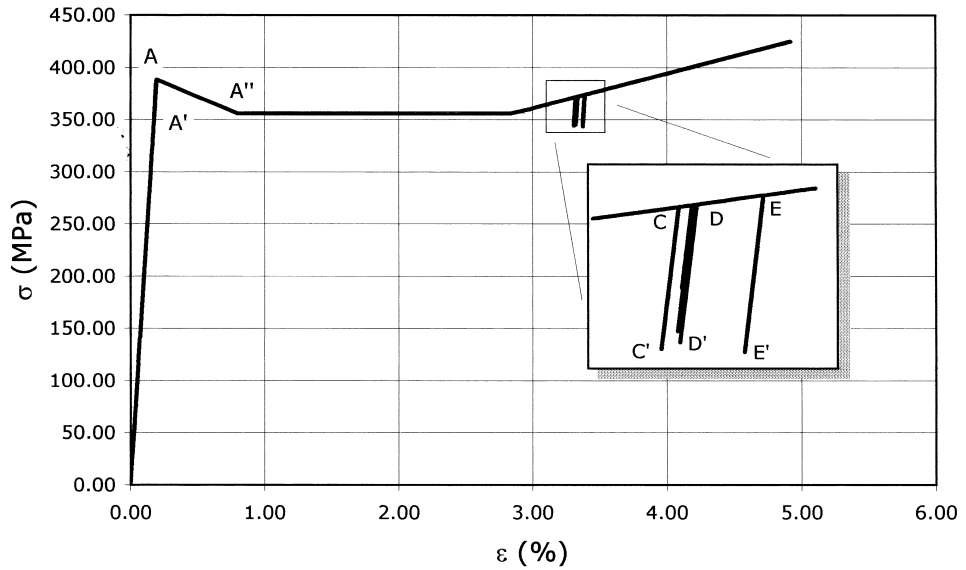

Fig. 10. Local stress–strain for element n. 80 (random-chain model).

which is practically twice that of Fig. 5, where each fall in stress corresponded exactly to the simultaneous yielding of *two* portions distributed symmetrically about the point where the first tooth broke.

A final characteristic feature concerns the local stress–strain diagrams, which are now of the type reported in Fig. 10. As compared to the graph in Fig. 7, the main difference resides in the elastic oscillations on the strain-hardening branch, which now occur following several (C-C′, D-D′, E-E′), rather than a unique (C-C′ in Fig. 7) loading-unloading path. This reflects the fact that, since the stress oscillations are not as regular as in Fig. 6, the generic element can now be unloaded at various stages of its strain-hardening phase. The analogy to Fig. 1b is immediate.

4. The influence of the loading device

The elastic energy stored in every testing machine renders *any* hard-device test an unattainable idealization. As mentioned in the Introduction, the influence of the loading device was first studied experimentally by Siebel and Schwaigerer (1937–1938) by inserting an elastic spring in series with the test specimen and varying its stiffness. They showed that the slope at which the stress falls from the upper yield point to a point on the plastic plateau of the stress–strain curve could be reduced by decreasing the constant $\Delta P/\Delta x$ of the elastic spring. In other words, the steepest slopes are obtained in machines which respond to load increases with the least relative movement between the two heads (hard-testing machine). As our previous results regard idealized situations, we feel it is important to render our analysis exhaustive by accounting for this effect as well.

In order to reproduce Siebel and Schwaigerer's experiment, we placed a linear elastic spring in series with the same uniform-chain-model bar discussed in Section 3a. Fig. 11 shows the local stress–strain

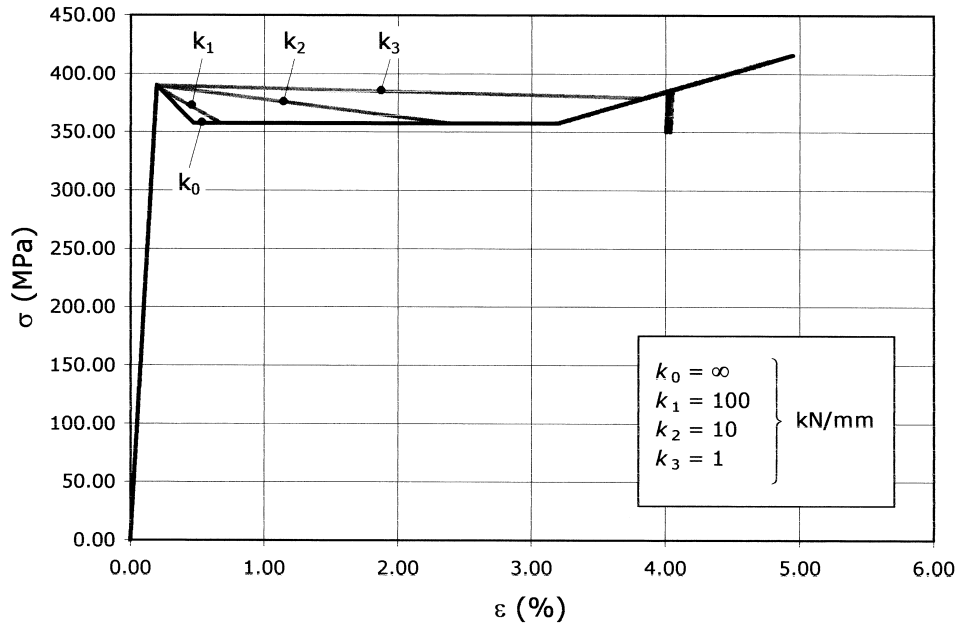

Fig. 11. Local stress–strain graphs for element number 80 (uniform-chain model for various elastic–constant values of the spring in series with the bar).

diagram for element n. 80, already considered above. The four descending branches correspond to different values of the spring's elastic constant: whereas $K_0=\infty$ coincides with the case of Fig. 7, we now consider the three values $K_1=100$ kN/mm, $K_2=10$ kN/mm and $K_3=1$ kN/mm. In particular, $K_1=100$ kN/mm is the measured stiffness of the machine used for our tests.

Siebel and Schwaigerer's conclusions can be readily interpreted within the framework of our model. When one retaining tooth fails, it is assumed that the piston P (Fig. 3a) slides instantaneously, producing a localized elongation and consequently releasing the elastic energy stored in all the bar elements. The piston must slide enough to produce a drop in load to a value of the order of F_l, which is compatible with the frictional constraint between the piston and cylinder. If an elastic spring is inserted in series with the bar, the softer the spring is, the greater this amount must be. The descending branches in Fig. 11 are fully covered by the piston stroke at the instant the retaining tooth breaks. In particular, when the softest spring of stiffness K_3 is inserted, the initial gap δ (Fig. 3) is completely closed after the retaining tooth breaks, and the representative point jumps directly onto the strain-

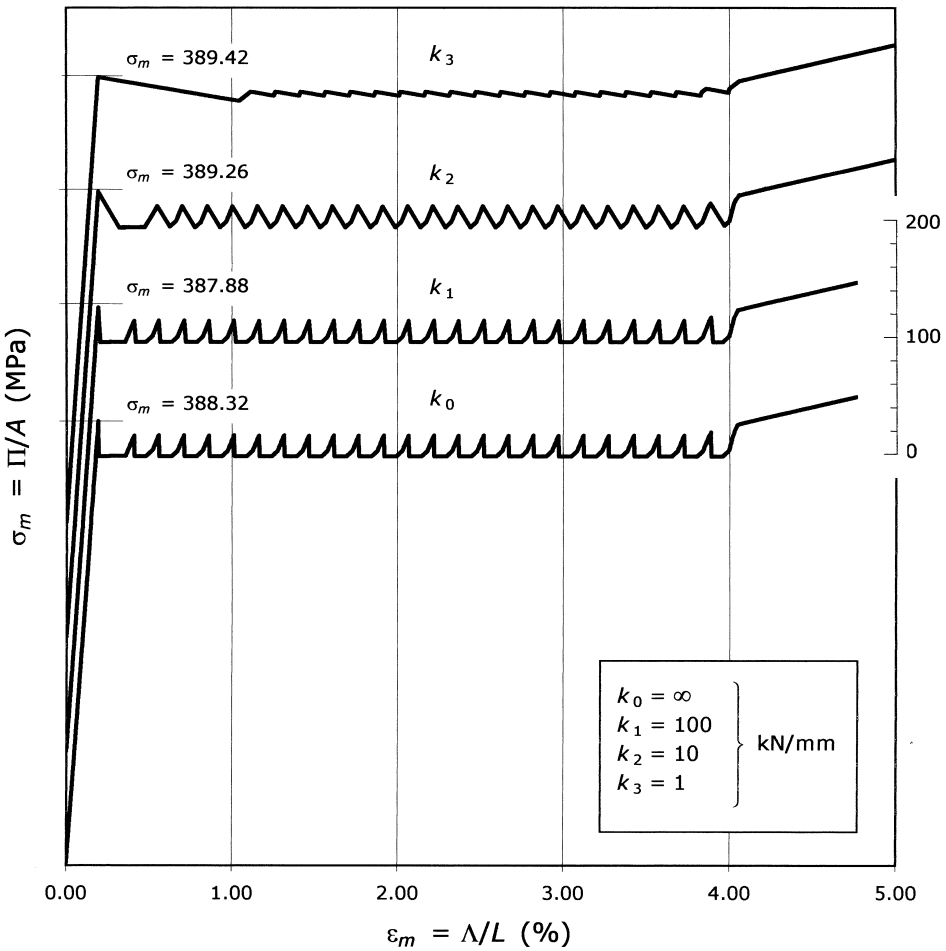

Fig. 12. Global stress–strain graphs of the uniform-chain model for various elastic–constant values of the spring in series with the bar.

hardening branch. This means that piston P comes into direct contact with the spring internal to the unit in Fig. 3.

Fig. 12 represents the global stress–strain diagrams obtained with the uniform-chain model for the four values K_0, K_1, K_2 and K_3. It is interesting to observe that the gradual decrease in testing machine stiffness translates into a smoothing out of the oscillations at the plastic plateau, thus confirming the experimental results of Miklowitz (1947) previously cited in the Introduction. In addition, the total number of oscillations may also be lowered, if the stiffness of the loading device is reduced sufficiently. In particular, whereas the wavelength of the oscillations remain essentially constant, some of the oscillations following the sharp yield point when the stiffness of the loading device is K_0 or K_1, tend to disappear when such stiffness is reduced to K_3. This is because the softer the loading device, the greater the amount of the elastic energy that must be released when the *first* tooth breaks. By comparing the diagram in Fig. 6 to that of Fig. 13, which presents the stress and local-strain histories with an in-series spring stiffness of K_3, we notice that here the elements involved during the first load drop are those from n. 52 to n. 64; i.e., this is what is required in order to render the bar axial force compatible with the loading capacity of the elementary units once their retaining tooth has broken.

Fig. 14 compares the average stress–strain curves obtained from the random-chain model already examined in Section 3 when the four loading-device stiffness values K_0, K_1, K_2 and K_3 are considered. The main difference we notice from Fig. 12 is that this time, not only the number, but also the wavelength of the oscillations may be affected. This is explained in Fig. 15, which shows the strain histories for the softer case, $K_3 = 1$ kN/mm. Due to the heterogeneity of the material properties throughout the bar, the number of units whose retaining teeth break simultaneously can vary considerably; this depends on the uneven distribution of weak points that the plastic wave encounters while travelling through the bar.

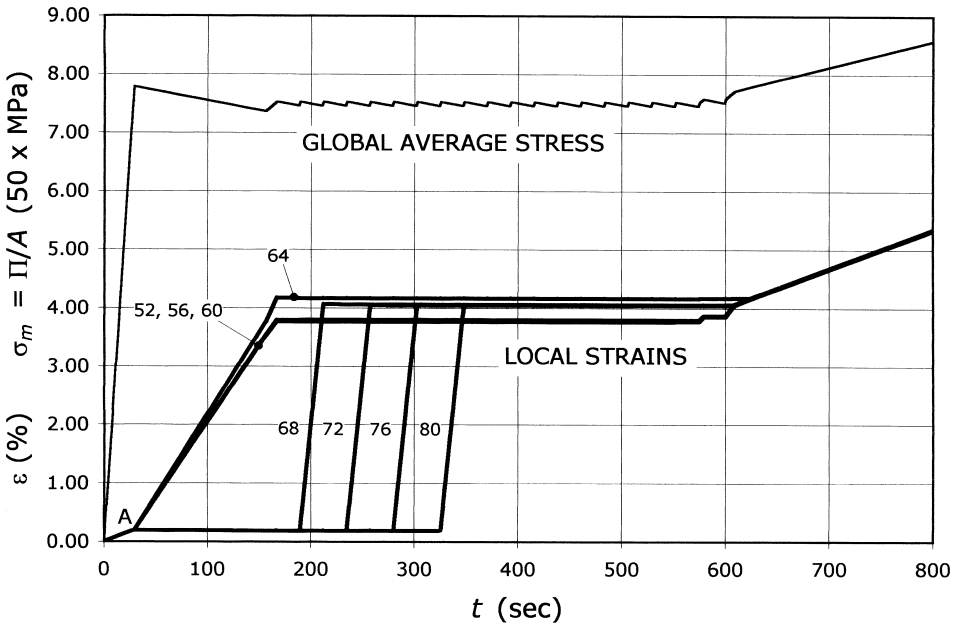

Fig. 13. Local strains and global average stress as functions of time for various elements in a uniform-chain model when the loading device has stiffness $K_3 = 1$ kN/mm.

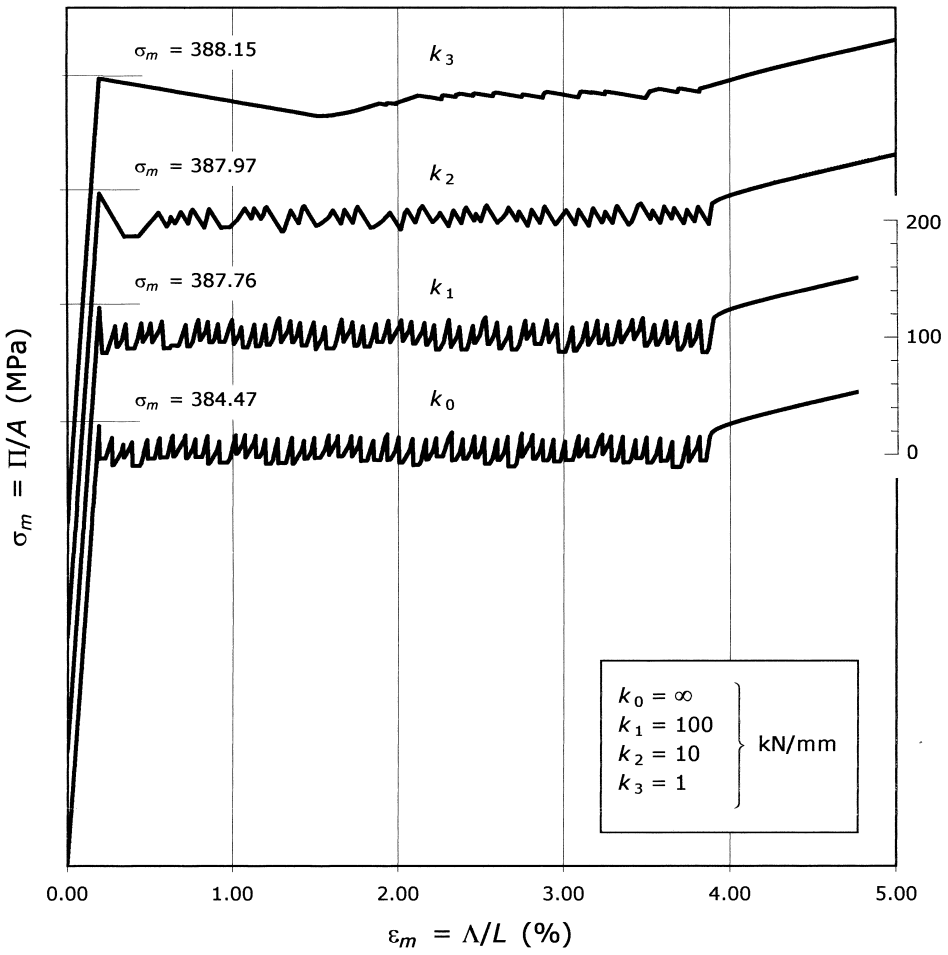

Fig. 14. Global stress–strain graphs of the random-chain model for various elastic–constant values of the spring in series with the bar.

In fact, it is noteworthy that the manner in which plastic deformations develop and advance through the formation of a plastic wave remains qualitatively the same, regardless of the stiffness of the inserted spring. This is another aspect that confirms our belief that the oscillations in the average diagram should not be attributed to the influence of the loading device.

As a final remark, the foregoing analysis also provides an objective criterion for judging whether the machine used for the experimental trials is to be considered hard or soft. As we are now in a position to compare, by means of Figs. 11, 12 and 14, the unattainable ideal situation ($K_0=\infty$) with that corresponding to the real, measured, stiffness ($K_1=100$ kN/mm), we evidence that the machine used for our tests can, with good approximation, be considered hard. The extent to which such an approximation can be deemed reliable is revealed by close scrutiny of the diagrams.

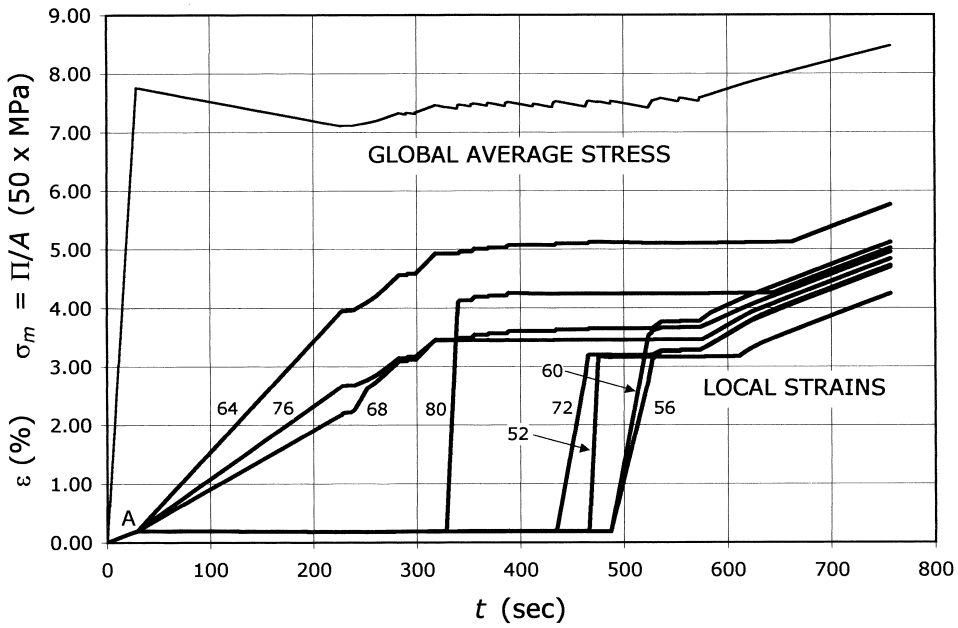

Fig. 15. Local strains as a function of time for various element in a random-chain model in a loading device of stiffness $K_3 = 1$ kN/mm.

Acknowledgements

The writers would like to express their most grateful appreciation to Mr Enrico Ulivieri for his skillful assistance in developing the numerical treatment of our model. The personal experience of Mr Luciano Pagni of the University of Pisa has been of great help in performing the experiments.

References

Bell, J.F., 1973. The experimental foundations of solid mechanics. In: Handbuch der Physik, vol. VIa/1. Springer-Verlag, Berlin.

Burns, T.J., 1994. A simple criterion for the onset of discontinuous plastic deformation in metals at very low temperatures. J. Mech. Phys. Solids 42, 797.

Carlson, J.M., Langer, J.S., 1989. Mechanical model of an earthquake fault. Phys. Rev. A 39, 6470.

Cottrell, A.H., 1961. Dislocations and Plastic Flow in Crystals, 4th ed. Clarendon Press, Oxford.

Davis, E.A., 1938. The effect of the speed of stretching and the rate of loading on the yielding of mild steel. ASME J. of Appl. Mech. 5, 137.

Dillon, O.W., 1966. Waves in bars of mechanically unstable materials. Journal of Applied Mechanics 33, 267.

Duleau, A.J.C., 1813. Essai thèorique et expérimental sur la résistance du fer forgé, (memoir presented to the French Academy, Paris).

Elam, C.F., 1938. The influence of the rate of deformation on the tensile test with special reference to the yield point in iron and steel. In: Proceedings of the Royal Society, London, 165, p. 568.

Ericksen, J.F., 1975. Equilibrium of bars. Journal of Elasticity 5, 191.

Froli, M., Royer-Carfagni, G.F. 1997. An experimental study of the Potervin-Le Chatelier effect in steel bars. In: Proceedings of the XIII National Meeting of AIMETA, Siena.

Froli, M., Royer-Carfagni, G.F., 1999. Discontinuous deformation of tensile steel bars: experimental results, ASCE. Journal of Engineering Mechanics 125 (12), 1243–1250.

Hanson, D., Wheeler, M.A., 1931. The deformation of metals under prolonged loading. Part I: the flow and fracture of aluminium. J. Inst. Metals, London 45, 229.
Korber, F., 1926. Zwanglose Mitteilungen des Deutschen Verbandes für Materialprüfung 8, 91.
Lempriere, B.M., 1962. Oscillations in tensile testing. Int. J. Mech. Sci. 4, 171.
Manjoine, M.J., 1944. The influence of rate of strain and temperature on yield stress in mild steel. Trans. Amer. Soc. Mech. Engrs. A-211.
Masson, A.P., 1841. Sur l'élasticité des corps solides. Annales de Chimie et de Phisique 3, 451 3rd series.
McReynolds, A.W., 1949. Plastic deformation waves in aluminium. Trans. Amer. Inst. of Mining and Metallurgical Engrs. 185, 32.
Miklowitz, J., 1947. The initiation and propagation of the plastic zone in a tension bar of mild steel as influenced by the speed of stretching and rigidity of testing machine. Journal of Applied Mechanics 14, A–31.
Müller, I., Villaggio, P., 1977. A model for an elastic–plastic body. Archive for Rational Mechanics and Analysis 102, 25.
Nadai, A., 1950. Theory of Flow and Fracture of Solids, vol. 1. McGraw-Hill, New York.
Portevin, A., Le Chatelier, F., 1923. Compte Rendu Acad. Sci. Paris 176, 507.
Rosenhain, W., Archbutt, S.L. 1912. Tenth report to the Alloys Research Committee: on the alloys of aluminium and zinc. In: Proceedings of the Inst. Mech. Engrs., p. 313.
Savart, F., 1837. Recherches sur les vibrations longitudinales. Annales de Chimie et de Phisique 65 2nd series.
Schmidt, W., 1995. Gleichmaßdehnung? Materialprüfung 37, 406.
Schulz, E.H., Buchholtz, H., 1926. Mitteillungen aus den Versuchsanstalten der Vereinigten Stahlwerke. Dortmunder Union Hörder Verein 2, 1.
Sharpe, W.N., 1966. The Portevin-Le Chatelier Effect in Aluminium Single Crystals and Polycrystals, PhD dissertation, The John Hopkins University, Baltimore, Maryland.
Siebel, E., Schwaigerer, S., 1937–1938. Die Streckgrenze beim Zugversuch unter besonderer Berücksichtigung des Einfluβes der Belastungsweise und der Machinenfederung. Archiv für das Eisenhüttenwesen, 11, 319.
Welter, G., Gockowski, S., 1938. Some fundamental factors regarding the stress–strain diagram of mild steel. Metallurgia 18, 61.
Wertheim, G., 1844. Recherches sur l'élasticité. Annales de Chimie et de Phisique 12, 385 3rd series.